Proceedings of the 34th European Modeling & Simulation Symposium (EMSS), 018
19th International Multidisciplinary Modeling & Simulation Multiconference

ISSN 2724-0029 © 2022 The Authors.
doi: 10.46354/i3m.2022.emss.018

Contact Resistance Influence in Numerical Simulation of Resistance Sintering

J.Amovin-Assagba[1], V.Bruyere[2,*], P.Namy[2], C.Durand[1] And S.Roure[1]

[1] SCHNEIDER ELECTRIC, EYBENS, France
[2] SIMTEC, 5 rue Felix Poulat, GRENOBLE France
*Corresponding author. Email address: vincent.bruyere@simtecsolution.fr

Abstract

Resistance sintering is a fast-sintering process used to compact and form a metallic part thanks to heat and pressure. To better control the geometry of the sintered material, a multi-physical model has been developed. To describe the current flow, the thermal exchanges and the mechanical aspects, this model requires the use of precise material properties as well as the knowledge of contact resistances. Indeed, these parameters are of first importance to describe the energy distribution in the system and the resulting metallurgical state. Different approaches have been compared in this work to study their influence on the values of interest. By considering the contact resistances as a function of pressure and temperature, this full 3D multi-physical approach offers a new tool to precisely predict the geometry of the resulting assembly.

Keywords: Sintering; Contact; Thermal Exchanges; Numerical Modeling; COMSOL Multiphysics

1. Introduction

Powder metallurgy associated with resistive sintering are used by Schneider Electric to produce electrical contacts. Thus, a cold-compacted silver-based part is at the same time sintered and assembled with its support thanks to Joule effect heating.

In switching and breaker products the contact material properties are keys for their reliability. Several silver-based material composites such as AgC, AgWC or AgSnO2 are used to get both good thermal and electrical conductivities and mechanical strength [Wintz et al,2013]. The choices of the powder mixing composition, the particle sizes and shapes are crucial to achieve the required properties. Associated with these choices, the resistance sintering-assembly of the contact parts – as called tips – is of a great importance to optimize their final properties. Thus, the final density, the hardness and the dimensions of the tips are very sensitive to the sintering conditions. And from the industrial point of view, those three elements are ones of the most relevant properties that illustrate the quality of the production.

Resistance sintering (RS) may achieve almost 100% dense tips within few seconds. The heating is mainly driven by the electrical and thermal contact resistances (ECR and ETR) between, on one hand the tip and the top electrode that brings the current and the pressure, and on the second hand the tip and its support (see Figure 1). The contact resistances – ECR and ETR – have been experimentally defined as functions of temperature at mean contact pressure.

As shown in [Feng et al.,2015] [Lopez et al.2011], numerical modeling offers opportunities for manufacturing development. Hence, we believe that numerical simulation of RS could be an interesting instrument to better understand the physical phenomena, to optimize the production cycles and the tools (geometry, material) and to guaranty the best tips properties. The model described here includes a full coupling between the three physics involved – electrical, thermal and mechanical – ones [Vanmeensel et al,2013; Manière et al,2016; Bourdon et al,2020].

Bulk conductivities are described according to a model that considers density and bonding-diffusion effects and their interdependence. The densification rate is calculated from a modified Norton–Green viscoplastic law retained to describe the mechanical behavior of the porous medium [Geslain et al,2018]. Creep tests on dense samples and sintering tests on porous ones have been achieved to complete the mechanical models for two materials AgC and AgWC.

In Section 2 of this paper, the modeling aspects are described. Geometry, operating conditions, and the equations solved in this work are detailed. The numerical strategy and the numerical validation of the model are explained in Section 3. The results obtained with different electrical and thermal contact resistances are finally discussed in Section 4.

2. Modeling

A description of the numerical model is developed in this section, based on a previous article [Bourdon et al,2020]. The major advance achieved in this work is the use of contact resistances as a function of local contact pressure and temperature to solve this highly coupled numerical problem. Only electrical and thermal phenomena are studied in detail here. Mechanical aspects and contact numerical algorithm are not described in this paper.

2.1. Geometry and operating conditions

The geometry is shown in Figure 1. A 2D axi-symmetrical assumption is used to simplify the model without losing any relevant information. It is composed of different parts: the electrode (in orange) and its holder (in yellow) where the current is applied at the top, and the tip (in dark purple), sintered and bonded on the support (in purple). At each interface in between parts, contact resistances are considered.

A high current and a compression load are applied from the electrode to the tip to densify the material and to obtain the required metallurgical and mechanical properties. Several physical phenomena are involved in the process, leading to a complex multi-physics problem.

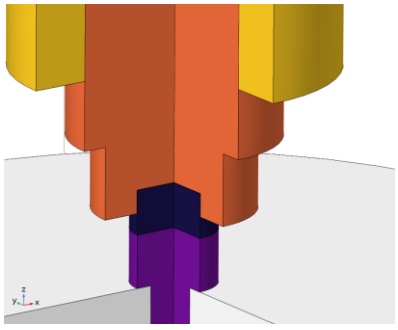

Figure 1. 2D axi-symmetrical geometry composed by the electrode (orange) and its holder (yellow), the tip (dark purple), the supports (purple and gray)

2.2. Equations and Boundary Conditions

To estimate the electric potential and the current in each part, the current conservation law is solved:

$$\nabla \cdot (\sigma \nabla V) = 0 \qquad (1)$$

where V is the electric potential and σ is the electrical conductivity of the material. The electric field $\boldsymbol{E}$ is defined by $\boldsymbol{E} = -\nabla V$.

A transient inward current density is applied at the top of the electrode. The ground reference is set at the bottom of the geometry. Electrical contact conditions are set at each interface to define the "electric potential jump" between the parts due to the imperfection of the contact. Indeed, at a microscopic level, contact is made at a finite number of spots defined by the local surface asperities. Furthermore, physicochemical state of the surfaces may also modify the contact resistance (see 2.3). A global approach is used here by writing the following relations to link the normal electric current density at the upside and downside boundaries:

$$\begin{aligned} \boldsymbol{n} \cdot \boldsymbol{J_1} &= \frac{1}{ECR}(V_1 - V_2) \\ \boldsymbol{n} \cdot \boldsymbol{J_2} &= \frac{1}{ECR}(V_2 - V_1) \end{aligned} \qquad \textit{Eq. 1}$$

where $\boldsymbol{J}_i = \sigma \boldsymbol{E}_i$ is the electric current density at each side of the interface and ECR is the electric contact resistance.

Due to the high current flowing through the metallic pieces and the contact junctions between them, thermal energy is generated inside the media and at the interfaces. The Joule effect inside the parts is taken into account as a source term, Q_{vol}, of the following energy equation:

$$\rho C_p \frac{\partial T}{\partial t} + \nabla \cdot [-k \nabla T] = Q_{vol} \qquad (2)$$

where T is the temperature, ρ the density, k the thermal conductivity, C_p the heat capacity of the material and Q_{vol} the resistive heat source term in the right-hand side of the equation, defined by:

$$Q_{vol} = \boldsymbol{J} \cdot \boldsymbol{E} \qquad (3)$$

As for the electric formulation, contact resistances are defined through the thermal point of view with the following relations between the heat fluxes:

$$\begin{aligned} \boldsymbol{n} \cdot \boldsymbol{q_1} &= \frac{1}{TCR}(T_2 - T_1) + \alpha \cdot Q_{surf,1} \\ \boldsymbol{n} \cdot \boldsymbol{q_2} &= \frac{1}{TCR}(T_1 - T_2) + (1 - \alpha) \cdot Q_{surf,2} \end{aligned} \qquad (4)$$

where $\boldsymbol{q_i}$ is the heat flux defined as $-k_i \nabla T_i$, TCR is the thermal contact resistance involved in the heat flux across the surfaces in contact, and α is the partition coefficient of the heat flux generated by Joule effect, expressed as:

$$Q_{surf,i} = \frac{1}{ECR} \cdot J_i^2 \quad (5)$$

A relation obtained from the literature (Charron, 1943) is used to estimate the partition coefficient between each surface:

$$\alpha = \frac{1}{1+\zeta} \quad with\ \zeta = \sqrt{\frac{\rho_1 \cdot C_{p_1} \cdot k_1}{\rho_2 \cdot C_{p_2} \cdot k_2}} \quad (6)$$

with k_i, ρ_i and $C_{p,i}$, the thermal properties of solid i.

This coefficient is thus equal to 0.5 if the same material is used for the two parts in contact. As for the other thermal boundary conditions, a reference temperature is applied at the bottom of the system, far from the heated area. Surface-to-ambient radiative conditions are applied for exterior boundaries to consider the radiative heat flux.

2.3. Contact Resistances

Depending on contact pressure, temperature, local roughness, and thermal properties, contact resistances are often very difficult to estimate precisely.

Different experimental and theoretical works have been devoted to problems related to interstitial contact conductance and to conductance by radiation [Cetinkale et al, 1951; Yovanovich et al, 1982]. In this work we only consider the thermal resistance, as the model is restricted to the case of surfaces in contact under conditions of negligible radiation [Song et al, 1992]. Many attempts at predicting thermal contact conductance, especially focusing on the contact pressure, have been made by using surface profile data. Mikic [Mikic, 1974] evaluates the thermal conductance $h_c^{thermal}$, assuming isotropic rough surfaces with circular contact points and gaussian distribution. To describe the surface conditions, the same approach from [Cooper et al, 1969] and based on the distribution of surface roughness height (σ) and surface roughness slope (m) is used here. The contact profile is thus described by the RMS value of the mean slope and the mean height of asperities on each surface:

$$m_{asp} = \sqrt{m_1^2 + m_2^2} \quad \text{and} \quad \sigma_{asp} = \sqrt{\sigma_1^2 + \sigma_2^2} \quad (7)$$

In accordance with many investigators [Greenwood et al, 1966; Mikic,1974], the thermal conductance can thereby be described as a function of the contact pressure, p, the thermal conductivity k_c, the contact elastic Modulus (E_c) and the RMS values of surface slope and height of asperities (m_{asp}, σ_{asp}) by:

$$h_c^{thermal} = 1.54 \cdot k_c \frac{m_{asp}}{\sigma_{asp}} \left(\frac{p\sqrt{2}}{m_{asp} E_c} \right)^{0.94} \quad (8)$$

with k_c, the equivalent thermal conductivity $\frac{2}{k_c} = \frac{1}{k_1} + \frac{1}{k_2}$, E_c, the equivalent elastic modulus $\frac{1}{E_c} = \frac{1-\nu_1^2}{E_1} + \frac{1-\nu_2^2}{E_2}$, with E_i the Young modulus and ν_i the Poisson's ratio of each material i in contact.

Finally, the contact resistance can be expressed as:

$$TCR = \frac{1}{h_c^{thermal}} \quad (9)$$

Concerning the electrical resistance, the same approach is used based on [Mikic, 1974]. It is obtained by replacing the equivalent thermal conductivity, k_c, in (eq.8) by the equivalent electrical conductivity, σ_c:

$$\frac{1}{ECR} = h_c^{\text{elec}} = 1.54 \cdot \sigma_c \frac{m_{asp}}{\sigma_{asp}} \left(\frac{p\sqrt{2}}{m_{asp} E_c} \right)^{0.94} \quad (10)$$

3. Numerical Strategy and Validation

The finite element method is used to solve all these equations together with a fully coupled approach in COMSOL Multiphysics® software. All described couplings and contact conditions form a highly non-linear problem requiring specific numerical solvers parameters. Concerning the time-scheme, a BDF algorithm is used by carefully tuning the timestep to ensure the precision of the results. To numerically validate our approach, mesh size and timestep influences have been studied in detail through heat and electric balance analyses. The results are shown in Figure 2. The electric power (in blue, Figure 2) is computed at the upper boundary, where the current density is applied with:

$$P_{elec} = 2\pi \int (\boldsymbol{J} \cdot \boldsymbol{n}) V r dr \quad (11)$$

The current density is set at the top, and thus the resulting power depends on the electrical resistances encountered by the current flow from the top to the bottom. Concerning the thermal powers, both volume source terms (in green, Figure 2) and at the contact interfaces (in red, Figure 2) are computed:

$$P_{Joule}^{Volume} = 2\pi \iint Q_{vol} r dr dz$$
$$P_{Joule}^{Surface} = 2\pi \int Q_{surf}\, r dr \quad (12)$$

To complete the balance, radiative losses are also estimated (in cyan, Figure 2).

$$P_{losses} = 2\pi \int \varepsilon\sigma (T^4 - T_{amb}^4) r dr \quad (13)$$

The sum of all thermal powers is calculated and represented with magenta markers in Figure 2. The total heat power generated in the model should be equal to the resulting total electrical power.

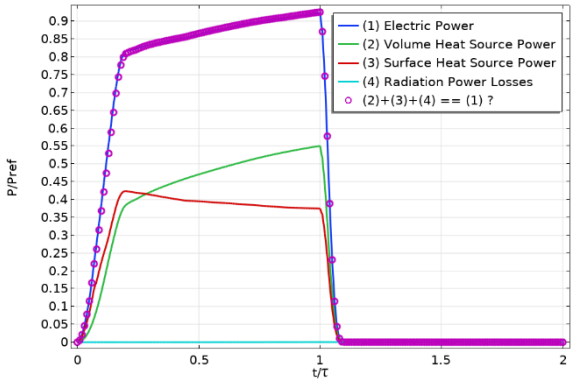

Figure 2. Electrical and thermal powers (non-dimensional) as a function of non-dimensional time where τ is the duration of the current application

As shown in Figure 2, the power is well balanced, with a maximum error lower than 0.5%, that numerically validates our approach.

The model can now be used to study the influence of different parameters as the electrical and thermal contact resistances.

4. Results

In a previous paper [Bourdon et al,2020], the ability of the model to predict residual stresses and final density in the tip has been presented. Mechanical aspects are not investigated here, and we mainly focus on the electrical and thermal exchanges.

Non-dimensional electric potential is plotted in Figure 3 in the different parts. Due to Electric Contact Resistances (ECR) between the different parts, discontinuities can be observed at the interfaces. The streamlines highlight the current flow through these boundaries. Concerning the temperature field, it is plotted in Figure 4, also emphasizing the discontinuity at the interfaces as well as the total heat flux (in arrows). The higher the Thermal Contact Resistance (TCR), the higher the Joule effect, which explains the maximum temperature in the tip. As shown in Figure 2, boundary and volume heat sources have the same order of magnitude and both contribute to the temperature increase. The characterization of the electrical and thermal contact resistances is thus of prior importance to estimate the resulting geometry and density of the tip.

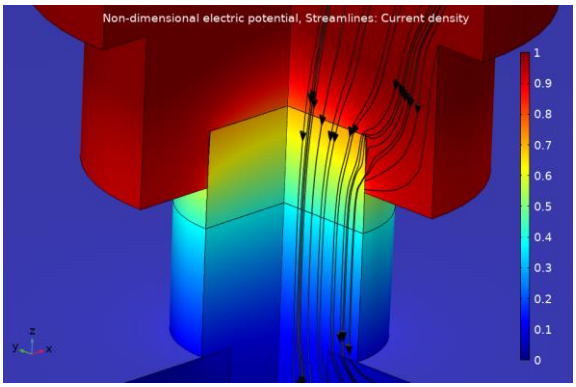

Figure 3. Non-dimensional electric potential and current density with streamlines at $t = \tau$

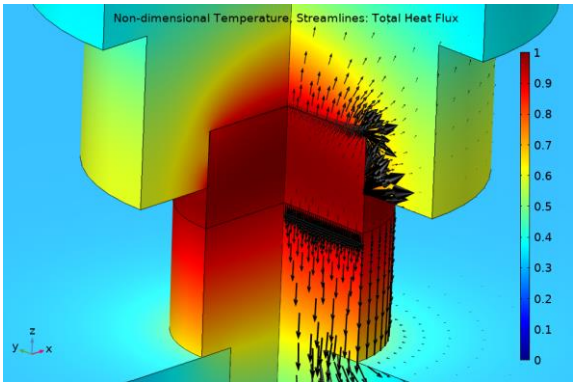

Figure 4. Non-dimensional temperature and total heat flux with arrows at $t = \tau$

Influence of Thermal Contact Resistances

The influence of TCR is studied here by comparing two different approaches. The first approach (without TCR(p)) consists in an estimation of the thermal resistance with experimental data at ambient temperature and under representative pressure load. For high temperature $\left(\frac{t}{\tau} > 0.25\right)$, an extrapolation is performed. The resulting mean TCR evolution can be seen in Figure 5 with markers, as a function of time, for the upper (blue) and lower (green) boundaries of the tip.

The mean TCR obtained with (eq.8) are plotted with solid lines in the same graph (Figure 5).

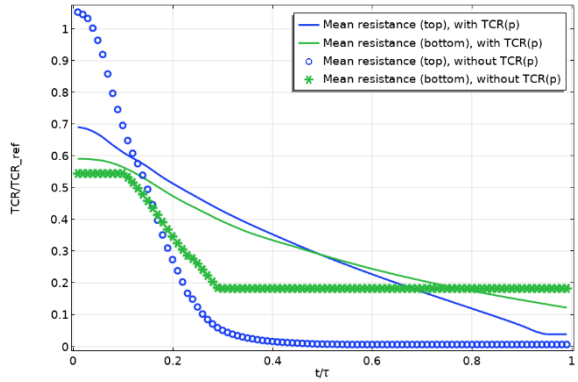

Figure 5. Non-dimensional temperature at the top centre (blue) and at the top periphery (green) of the tip with and without TCR function of the contact pressure

First, it can be seen in Figure 5 that the order of magnitude is the same for both approaches. At the beginning of the process, the values of the resistances are high and then decrease due to high pressure and temperature. The evolution is more linear for the case where the pressure and temperature variations are considered. Indeed, for the first approach (markers), the extrapolation is constant at high temperature.

To study the influence on the resulting thermal state in the tip, two points of interest are defined. The first one is located at the top center of the tip, the second one at the top periphery of the tip. The temperature evolution is plotted for these two points as a function of time in Figure 6.

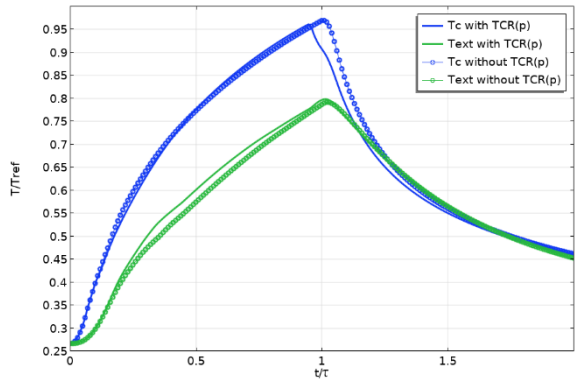

Figure 6. Non-dimensional temperature at the top centre (blue) and at the top periphery (green) of the tip with and without TCR function of the contact pressure

No major effect is observed in Figure 6 concerning the TCR influence. Indeed, the order of magnitude of TCR for both approaches (with or without considering the local pressure) is the same and the impact on thermal kinetics is thus negligible.

Influence of Electric Contact Resistances

The influence of ECR is studied in this section. Their effects are more important because they directly affect the thermal source term *via* the Joule effect. Their evolution as a function of time is plotted in Figure 7 as they are for the TCR study. The temperature evolution is plotted in Figure 8 for both approaches at the two points of interest.

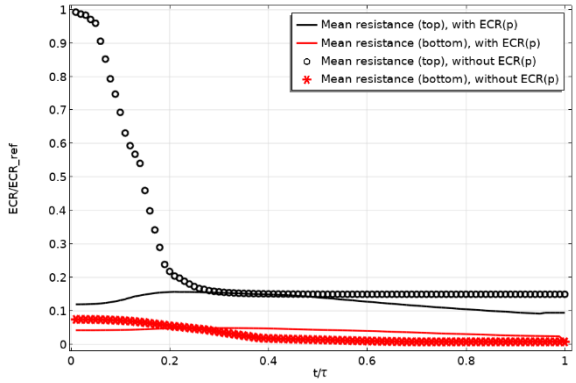

Figure 7. Non-dimensional ECR at the top centre (black) and at the top periphery (red) of the tip with and without ECR function of the contact pressure

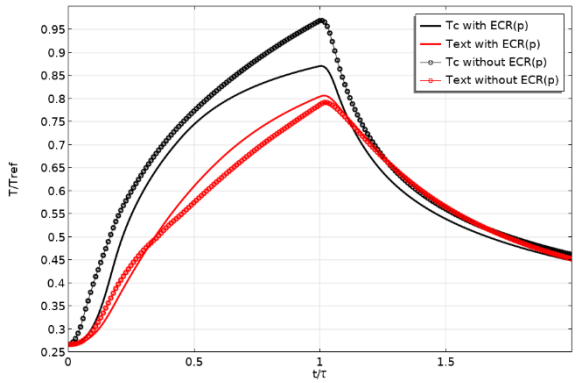

Figure 8. Non-dimensional temperature at the top centre (black) and at the top periphery (red) of the tip with and without ECR function of the contact pressure

In Figure 7, the ECR values reached at high temperature $\left(\frac{t}{\tau} > 0.25\right)$ appear to be very close for both approaches. For lower temperature $\left(\frac{t}{\tau} < 0.25\right)$, the calculated ECR (black solid line) are lower than the experimental and extrapolated ones (black markers) for the top surface of the tip due to weak variations of pressure and weak influence of the temperature evolution. The resulting thermal state (Figure 8) is slightly affected by these variations and as expected, the temperatures are lower for the lower resistances (with ECR(p)). In Figure 7 and Figure 8, the order of magnitude of the numerical estimation of ECR as a function of pressure is in good agreement with the experimental measurements. This suggests the technique could be used for different materials in further studies.

To finalize this study, two resulting density states obtained with and without ECR(p) and TCR(p) are compared in Figure 9.

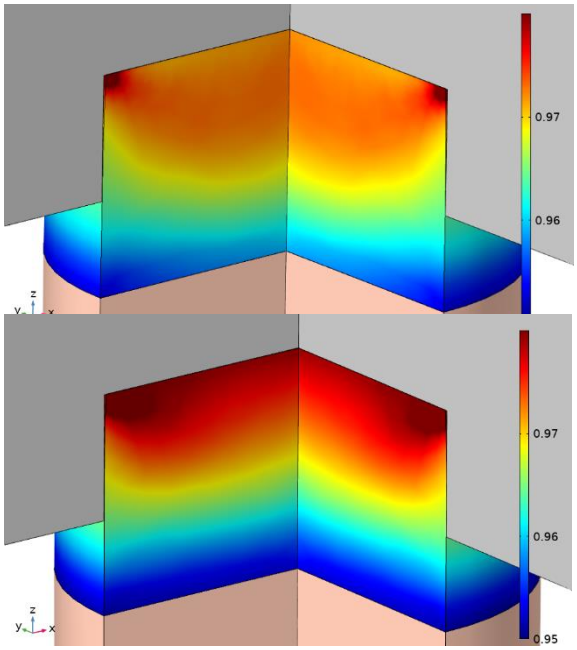

Figure 9. Non-dimensional density for both approaches: with TCR(p) and ECR(p) (at the top) and without TCR(p) and ECR(p) (at the bottom)

The mean values of density appear to be very close for both cases (Figure 9). Concerning the density distribution, slight differences are observed at the top because of a different thermal state and local contact resistance differences between both approaches. Nevertheless, the approach proposed here to estimate the ECR and TCR is very promising. Indeed, we can now:

- ➔ predict the ECR and TCR as a function of the local pressure for different materials and use our model for other types of contact,
- ➔ consider the local contact pressure variations in the model to predict more precisely the resulting density of the tip.

5. Conclusions

A Multiphysics model has been developed in this work including, among other aspects, the variations of contact resistances with local contact pressure. The strongly coupled problem - mechanical behavior laws and contact, electrical and thermal exchanges - has been solved through a fully coupled approach. The results have been compared with TCR and ECR values obtained experimentally at a constant pressure and with a relation from the literature related to the local contact pressure. Good agreement has been found for TCR and ECR values as a first evaluation. More precisely, some differences have been investigated through local density evolution, leading to a better understanding and a better control of this process. This predictive model can now be used to study the influence of each operating condition (power, force, duration...), and gives some valuable information about the robustness of the process. Furthermore, by now estimating the TCR and ECR with material properties only (local roughness, stiffness, electrical and thermal properties), different materials and geometries could be numerically studied to optimize the design of the process.

References

Z. Feng, H. Champliaud, (2015), Modeling and Simulation based on Finite Element Method for Electron Beam Welding, Proceedings of the European Modeling and Simulation Symposium, 2015.

A. López, J. A. Somolinos, L. R. Núñez, A. M. Carneros (2011), Simulation of Gesmey Generator Manouevers, Proceedings of the European Modeling and Simulation Symposium, 2011.

J.L. Wintz, S. Hardy, (2013), Design guideline of contactors: Optimal use of assembled contacts, Holm Conference on Electrical Contacts (HOLM), IEEE 59th, p 1-6. https://doi.org /10.1109/HOLM.2014.7031014

K. Vanmeensel , A. Laptev, H. Sheng, I. Tkachenko, O. Van der Biest, J. Vleugels, (2013), Experimental study and simulation of plastic deformation of zirconia-based ceramics in a pulsed electric current apparatus, Acta Materialia 61 2376–2389

C. Manière, U. Kus, L. Durand, R. Mainguy, J. Huez, D. Delagnes, C. Estournès, (2016), Identification of the Norton-Green Compaction Model for the Prediction of the Ti–6Al–4V Densification During the Spark Plasma Sintering Process, Advanced Engineering Materials, Vol 18, Issue 10, p 1720-1727.

S. Bourdon, V. Bruyère, P. Rogeon, P. Namy, C. Durand, S.Roure, (2020), Numerical Simulation Of Electro-Thermo-Mechanical Phenomena During Resistance Sintering, Comsol Conference 2020.

E. Geslain, P. Rogeon, T. Pierre, C. Pouvreau, L. Cretteur, (2018), Coating effects on contact conditions in resistance spot weldability, Journal of Materials Processing Technology, Volume 253, March 2018, Pages 160-167.

F. Charron, (1943), "Partage de la chaleur entre deux corps frottants," *Publication Scientifique et Technique du Ministère de l'Air*, no. 182.

T. Cetinkale and M. Fishenden, (1951), «Thermal conductance of metal surface in contact », Proceeding of general discussion on heat transfer, p.271à-275.

M. Yovanovich, J.W DeVaal, (1982), «A statistical model to predict thermal gap conductance between conforming rough surfaces» 3rd joint thermophysics, fluids, plasma and heat transfer

conference, June 7-11, St-Louis, Missouri.

S. Song, M. Yovanovich, (1992) «Thermal gap conductance : Effects of gas pressure and mechanical load», AIAA 27 the Aerospaces meeting.

B. Mikic, (1974), *Thermal contact resistance; Theoretical considerations*, Department of Mechanical Engineering, Massachusetts Institute of Technology, Int J. Heat Mass Transfer. Vol. 17, pp. 205-214.

M. Cooper, B. Mikic, M. Yovanovich (1969), Thermal contact conductance, Int J. Heat Mass Transfer. Vol. 12, pp. 279-300.

J. A. Greenwood and J. B. P. Williamson (1966), Contact of nominally flat surfaces. Proc. R. Sot.. Lond. 295, 300- 319.